Improved Adhesion of Different Environmental Barrier Coatings on Al₂O₃/Al₂O₃-Ceramic Matrix Composites

Caren Gatzen,* Daniel Emil Mack, Olivier Guillon, and Robert Vaßen

In high-temperature combustion atmospheres, well-adhering environmental barrier coatings (EBCs) are required to protect the underlying ceramic matrix composites (CMCs) from corrosion. Herein the adhesion mechanisms of three different coatings produced by atmospheric plasma spraying (APS) on an Al₂O₃/Al₂O₃-CMC are investigated. In particular, the influence of surface structuring by laser ablation prior to coating production is investigated. Y_2O_3, yttria-stabilized zirconia (YSZ), and $Gd_2Zr_2O_7$ are chosen as potential EBCs. The coating adhesion on CMC-substrates with and without surface structuring is analyzed by furnace cycling, pull-adhesion tests, and burner-rig tests with gradient. Special interest is paid to the interactions at the coating–substrate interface before and after heat treatment and their effect on the coating adhesion and lifetime. Two different adhesion mechanisms are found: adhesion promoted by chemical reaction and adhesion promoted by mechanical interlocking.

1. Introduction

Among other things, the efficiency of a gas turbine is limited by its maximum service temperature, which is determined by the thermomechanical capabilities of the components in the high-temperature section of the turbine. Decades of research are therefore aiming for solutions that enable a further increase in the turbine inlet temperature. In the past years, the maximum service temperature could be drastically increased by the use of thermal barrier coatings (TBCs) and complex cooling systems. Unfortunately, the extra work that is needed for cooling causes high-efficiency losses. Calculations showed that operation at 1300 °C without cooling could increase the output power by almost 50%.[1,2] Another factor, especially relevant to applications

in aviation, is the reduction of weight. Any weight reduction reduces fuel consumption not only by the amount of the original mass which does not need to be accelerated, but also by the mass of the saved fuel. Therefore, the desire to further optimize the process generates the demand for lighter materials with a higher thermomechanical stability compared with the single-crystal superalloys that are frequently used up to now.

Ceramic matrix composites (CMCs) based on oxides, for example, alumina, are suitable materials to meet the increasing requirements for high-temperature applications in gas turbine environment. This is due to their excellent temperature stability,[3,4] as well as due to their reduced weight compared with current state-of-the-art nickel-based alloys. Although alumina is quite inert, water vapor that is present in the aggressive turbine atmosphere ($\approx$10%)[5,6] can cause severe corrosion, as it leads to the formation of volatile hydroxides at temperatures above 1200 °C.[7] Therefore, the application of suitable environmental barrier coatings (EBC) to mitigate this corrosion is inevitable for long-term use.

$$Al_2O_{3(s)} + 3H_2O_{(g)} \rightleftharpoons 2Al(OH)_3(g) \tag{1}$$

Obviously, the ideal EBC should have high corrosion resistance and should be stable at high temperatures. To identify potential EBC candidates, corrosion rates of several materials have been studied.[8–14] Water vapor corrosion rates of an Al₂O₃/Al₂O₃-CMC and possible coating materials are shown in **Table 1**. In addition to a high water vapor resistance, a dense microstructure is preferred to suppress the diffusion of water through the coating. However, a dense coating can cause high stresses during thermal cycling, leading to premature failure. To achieve a long service life, a low coefficient of thermal expansion (CTE) mismatch between coating and substrate is advantageous. Considering that, materials such as Y_2O_3 and yttrium aluminates appear to be more suitable than yttria-stabilized zirconia (YSZ) and $Gd_2Zr_2O_7$.

The suitability of Y_2O_3 as EBC for oxide-based WHIPOX CMCs has been studied by Mechnich et al. and was also demonstrated on real combustor components.[23,24] Prior to coating by atmospheric plasma spraying (APS), a reaction-bonded aluminium oxide (RBAO) bond coat was applied to increase the adhesion of the coatings to the substrate and reduce the gas permeability of the sample.[25] The formation of a reaction layer consisting of the series of yttrium aluminates ($Y_4Al_2O_9$, $YAlO_3$,

Dr. C. Gatzen, Dr. D. E. Mack, Prof. O. Guillon, Prof. R. Vaßen
Institute of Energy and Climate Research
Forschungszentrum Jülich GmbH
52425 Jülich, Germany
E-mail: c.gatzen@fz-juelich.de

Prof. O. Guillon
JARA-Energy
Jülich Aachen Research Alliance
Jülich, Germany

The ORCID identification number(s) for the author(s) of this article can be found under https://doi.org/10.1002/adem.202000087.

ADVANCED
SCIENCE NEWS

www.advancedsciencenews.com

ADVANCED
ENGINEERING
MATERIALS

www.aem-journal.com

Table 1. CTEs and corrosion rates of an Al_2O_3/Al_2O_3-CMC and relevant EBC candidates. Positive values indicate a mass loss during corrosion test. Negative values correspond to a mass gain during corrosion test.

Material	Coefficient of thermal expansion [10^{-6} K^{-1}]	Corrosion rate [mg cm^{-2} h^{-1}]
Al_2O_3/Al_2O_3-CMC	8.5[15]	2.14[16]
Y_2O_3	8.5[17]	1.22×10^{-2}[18]
YSZ	11.7[19]	2.39×10^{-2}[11]
$Gd_2Zr_2O_7$	12.4[20]	-5.0×10^{-3}[21]
$YAlO_3$	7.53[10]	8.0×10^{-4}[10]
$Y_3Al_5O_{12}$	9.23[10]	2.1×10^{-3}[10]
$Y_4Al_2O_9$	7.3[22]	-7.1×10^{-4}[10]

and $Y_3Al_5O_{12}$) was observed after exposure to high temperatures. As the yttrium aluminates have similar CTEs compared with coating and substrate, the reaction layer was classified as not detrimental. On the contrary, the good bonding between coating and substrate was attributed to the formation of a reaction scale.[23] Recently, water vapor corrosion tests of an Y_2O_3-coated Al_2O_3/ Al_2O_3-CMC demonstrated its high potential as EBC.[16]

Following the arguments of well-matching CTEs, the yttrium aluminates $Y_3Al_5O_{12}$ and $YAlO_3$ are promising coating candidates as well. However, it is known from literature that the application of yttrium aluminate coatings by APS is quite challenging.[26,27] This is due to the unfavorable volume shrinkage of partially amorphous coatings during recrystallization. In a recent study of $YAlO_3$ EBCs on Keramikblech FW12, we demonstrated that problems such as phase segregation and pore formation can be overcome using very low pressure plasma spraying (VLPPS).[26] Using low-pressure conditions, well-molten and fast particles, as well as higher substrate temperatures and lower cooling rates, can be achieved, resulting in dense and fully crystalline coatings. Similar to the Y_2O_3 coatings, the formation of a reaction layer between EBC and alumina-based CMC substrate was observed. In contrast to the APS process, in the VLPPS process, the formation of a reaction scale was observed directly after spraying. Pull-adhesion tests (PATs) showed that the adhesion of $YAlO_3$-VLPPS coatings was significantly higher than for APS coatings, which lacked a reaction layer. Therefore, it is likely that the good coating adhesion can be associated with the formation of reaction scale at the coating–substrate interface. Furthermore, VLPPS-$YAlO_3$ coatings showed a long service life in burner-rig tests with temperature gradients. It should be noted that no additional bond coats or surface treatments were required in our study.

The impact of the reaction scale at the coating–substrate interface on the coating adhesion/lifetime is especially interesting in the context of $Gd_2Zr_2O_7$ coatings. $Gd_2Zr_2O_7$ is a commonly used material in the TBC area and is known for its high resistance against fly ash attack.[28] As the material has already been well-investigated and a resistance against steam and hot corrosion was found, it is an interesting candidate for EBCs despite its large CTE mismatch ($\Delta_{CTE} \simeq 3.9 \times 10^{-6}$ K^{-1}). Studies in the TBC area showed that a reaction between Al_2O_3 and $Gd_2Zr_2O_7$ to $GdAlO_3$ can occur.[21,29,30] In contrast to the EBCs where a reaction of

Y_2O_3 or yttrium aluminate coatings with the substrate is considered to promote adhesion, the formation of $GdAlO_3$ at the Al_2O_3– $Gd_2Zr_2O_7$ interface was associated with premature failure of the coating. For this reason, there are only few studies concerning $Gd_2Zr_2O_7$ as EBC. Recently, Gatzen et al.[31] showed that the coating application of $Gd_2Zr_2O_7$ coatings on Al_2O_3/Al_2O_3-CMCs (Keramikblech FW12) by APS is possible. However, the coating adhesion on untreated substrates was quite poor which was explained by bad wetting behavior of the coating. The adhesion was drastically increased by surface roughening using laser ablation. Contrary to the experiments with $YAlO_3$, no reaction between coating and substrate was observed directly after spraying.[32] Because no high-temperature tests were conducted, whether a potential reaction at the interface favors adhesion remains unanswered.

Another material known in the TBC field is YSZ. Unlike $Gd_2Zr_2O_7$, Y_2O_3, and the yttrium aluminates, no reaction between YSZ and the alumina-based substrate is expected. Despite its rather high CTE mismatch ($\Delta_{CTE} \simeq 3.2 \times 10^{-6}$ K^{-1}), YSZ was tested for its suitability as an EBC, e.g., by Gerendás et al.[33] and Mechnich et al.[34–36] The latter showed the promising performance of YSZ coatings produced by electron-beam physical vapor deposition (EB-PVD). Nevertheless, the WHIPOX substrates used in that study had to be pretreated by sandblasting or grinding to ensure a good bonding; afterward, an RBAO[37] bond coat had to be applied to improve the coating adhesion. Gerendás et al.[33] reported a surprisingly long lifetime of APS-YSZ coatings on sandblasted UMOX substrates. In contrast to this, significantly shorter lifetimes were found for YSZ coatings on sandblasted WHIPOX and OXIPOL substrates. This result demonstrates that the results cannot be easily transferred from one coating–substrate system to another. Therefore, the question remains whether YSZ is a suitable EBC candidate for the CMC (Keramikblech FW12) used in this study and whether a surface treatment, respectively, which one, can be applied.

However, Vaßen et al.[32] showed recently that mechanical treatment of the brittle ceramic matrix in CMCs may lead to severe damage and premature coating failure. It was suggested to use surface structuring by laser ablation instead. Another suggested option is the usage of an APS-Y_2O_3 layer as bond coat.[32] Summarizing , we can say that the formation of reaction layers at the interface, as the examples of Y_2O_3 and $YAlO_3$ show, may have a positive effect on the adhesion of the coating. Experiments with coatings where no reaction is possible, such as YSZ, show that good surface pretreatment is necessary to increase adhesion. A good substrate pretreatment may allow the use of materials with moderate CTE mismatch. If possible, a method that is not harmful to the substrate should be chosen, such as laser ablation.

Some questions, however, arise from these observations which are as follows:

1) Is it possible to further increase the adhesion of coatings that form a reaction scale (e.g., Y_2O_3) by laser structuring of the substrate?

2) Does the increased adhesion at room temperature arising from surface structuring by laser ablation also lead to a sufficient service life in burner-rig tests, especially for coatings with a higher CTE mismatch (e.g., $Gd_2Zr_2O_7$ and YSZ)?

**ADVANCED
SCIENCE NEWS**

www.advancedsciencenews.com

**ADVANCED
ENGINEERING
MATERIALS**

www.aem-journal.com

3) Does thermal cycling of $Gd_2Zr_2O_7$ coatings lead to the formation of a reaction scale? If so, will this result in increased adhesion or premature failure of the coating?

Experiments in this study aim to answer these questions. For this, a commercially available alumina-based CMC (Keramikblech FW12) was coated by APS. Y_2O_3, $Gd_2Zr_2O_7$, and YSZ coatings were chosen as coating materials. For a better understanding of the adhesion mechanism, some samples were subjected to a surface pretreatment by laser ablation prior to coating application. Samples with and without laser structuring were coated with each coating material. PATs, furnace cycling tests, and burner-rig tests with gradient were conducted to study the coating adhesion. The samples were analyzed by means of X-ray diffraction (XRD) and scanning electron microscopy (SEM). By comparing materials with different potentials to form reactions with the substrate and with clearly different CTE mismatches, it should be possible not only to answer the aforementioned questions, but also to clarify the interaction of the different adhesion mechanisms.

2. Experimental Section

The CMC used for this study was the commercially available material FW12 (Pritzkow Spezialkeramik, Germany), consisting of alumina fibers (Nextel 610) that are embedded in a porous matrix of 85% alumina and 15% YSZ. All samples were ultrasonically cleaned before coating application.

A Nd:YAG laser with a wavelength of 1062 nm and a maximum peak power of 15 kW was used for the surface structuring of the substrate. Two different surface structures were chosen for surface structuring (**Table 2**). The surface structuring is described in detail in a previous study.[31]

Different coating materials were chosen as EBC: Y_2O_3, $Gd_2Zr_2O_7$, and YSZ. APS was used for coating manufacture; the coating parameters are shown in **Table 3**. An Oerlikon Metco MultiCoat facility was used, equipped with a TriplexPro-210 gun that was mounted on a six-axis robot. The substrate temperatures during the coating procedure were measured with an IR pyrometer.

Spray-dried powders were used for coating manufacture (**Table 4**). The XRD measurements of the powders are shown in **Figure 1**. The measurements reveal the high purity of the used

Table 2. Used laser parameters.

Structure	Pulse per point	Spot distance [μm]
Mixed	50	45
Dot	50	100

powders. The coated samples were furnace cycled in air for 4×20 h at 1200 °C. XRD measurements were conducted before and after thermal aging. A Bruker D4 Endeavor (Karlsruhe, Germany) with Cu Kα radiation ($\lambda = 1.54187$ Å) was used for XRD measurements.

Coating adhesion of as-sprayed coatings was measured by PATs. For this, an Elcometer 510 (Aalen, Germany) was used according to ASTM D4541. Test dollies with 10 mm diameter were glued to the coated surface with an Araldite two-part epoxy adhesive.

The coating performance during thermal cycling with a thermal gradient was tested by burner-rig tests, and the used setup is described by Traeger et al.[42] The samples were mounted in a ceramic sample holder and subjected to cycles of 5 min of heating followed by 2 min of cooling. The temperature was measured with pyrometers from the front and back side. The used temperature program consisted of 510 cycles at 1200 °C, followed by 500 cycles at 1300 °C, followed by 230 cycles at 1400 °C. The backside temperature was set to 600 °C.

Materialographic cross sections were prepared from samples in the as-sprayed state and after testing. The polished samples were sputtered with platinum (Leica EM ACE200, Vienna, Austria) and analyzed by SEM (Hitachi, TM3000).

3. Results and Discussion

3.1. Coating Formation and Interface Reactions

First, the cleaned CMC substrates were coated without additional pretreatment. XRD measurements of the as-sprayed and heat-treated samples are shown in **Figure 2**. The coatings are highly crystalline and phase pure even in the as-sprayed state. The measurements show no significant difference between the as-sprayed and heat-treated state. Therefore, neither crystallization nor phase transformation are expected to take place during heat treatment. The diffraction pattern of $Gd_2Zr_2O_7$-coated samples shows the presence of traces of ZrO_2 and Gd_2O_3. During plasma spraying, Gd is vaporized, changing the stoichiometry of $Gd_2Zr_2O_7$ and causing demixing. This phenomenon is well known for this material.[46]

A typical Y_2O_3 splat is shown in **Figure 3**a. The splat has a disk-like shape, which is characteristic for the ideal splat morphology, indicating a good wetting behavior of the coating–substrate system.[47,48] Therefore, smooth and good adherent coatings are expected. In contrast to this, the splat of the YSZ coating (Figure 3b) is not well flattened and unmolten/partial molten parts can be observed. The presence of unmolten particles can be attributed to the larger particle size of YSZ powder, compared with Y_2O_3 and $Gd_2Zr_2O_7$ powders. The low flattening indicates

Table 3. Used coating parameters for the production of APS coatings (SLPM = standard liter per minute).

	Distance [mm]	$T_{Preheat}$ [°C]	$T_{Coating}$ [°C]	Current [A]	Ar [SLPM]	He [SLPM]	Carrier gas [SLPM]	Passes	Thickness [μm]
Y_2O_3	120	450	620	520	46	4	4.5	6	240
$Gd_2Zr_2O_7$	120	500	600	520	46	4	2	10	270
YSZ	200	150	300	420	46	4	2	15	360

Table 4. Characterization of used powders.

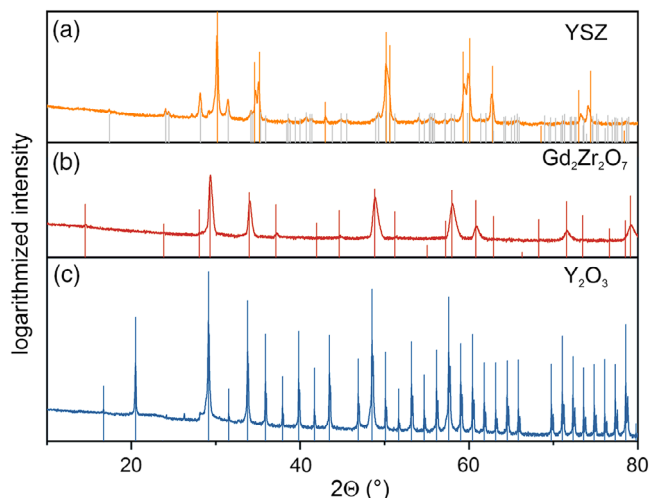|	Manufacturer	Particle size [µm]
Y_2O_3	Oerlikon Metco	30
$Gd_2Zr_2O_7$	IEK-1	32
YSZ	Oerlikon Metco	54

Figure 1. Logarithmized XRD measurements of used powders. a) Diffraction pattern of YSZ (orange) with reference patterns for tetragonal ($P4_2nmc$, orange)[38] and monoclinic ($P2_1/c$, gray)[39] modifications. b) XRD measurement of $Gd_2Zr_2O_7$ (red) with reference pattern for pyrochlore modification ($Fd\bar{3}m$, red).[40] c) Measured diffraction pattern of Y_2O_3 (blue) with reference pattern[41] ($Ia\bar{3}$, blue).
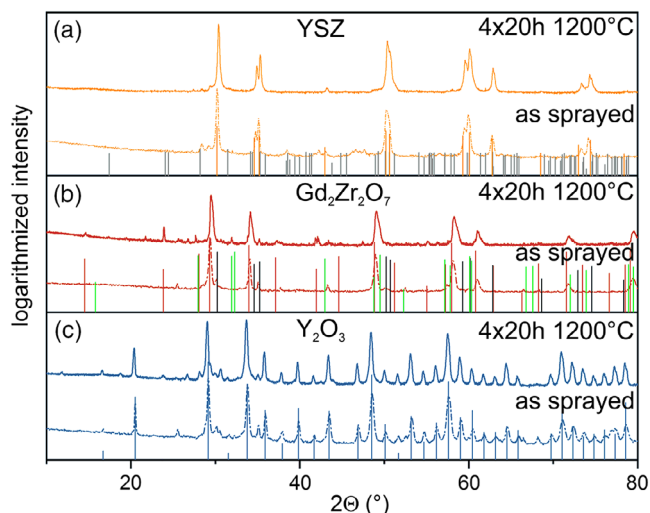

Figure 2. XRD measurement of obtained coatings after spraying (dotted line) and after furnace cycling (solid line). a) XRD measurements of YSZ (orange) and reference patterns for tetragonal ($P4_2nmc$, orange)[38] and monoclinic ($P2_1/c$, gray)[39] modifications. b) XRD measurements of $Gd_2Zr_2O_7$ coatings (red), reference line pattern for pyrochlore $Gd_2Zr_2O_7$ ($Fd\bar{3}m$, red),[40] Gd_2O_3 ($P\bar{3}m1$, green),[43] and ZrO_2 ($P4_2/nmc$, black)[44] were added. c) Measured diffraction pattern for Y_2O_3-coated samples (blue) and reference pattern ($Ia\bar{3}$, blue);[41] remaining peaks can be attributed to monoclinic[45] Y_2O_3 ($C2/m$).

poor wetting and thus bad contact between coating and substrate. The reduced flattening can be explained by the incomplete melting and the lower substrate temperature during thermal spraying.[49–51] As a result of the worse contact and the lower degree of melting, a weak adhesion and higher porosity of YSZ coatings is expected. The SEM image of the $Gd_2Zr_2O_7$ splat is shown in Figure 3c. The splat is irregular shaped and cracked. The high CTE difference between $Gd_2Zr_2O_7$ and substrate causes high stresses during quenching, leading to partial delamination of the splat. A reduced level of adhesion is, therefore, expected.

SEM images of the coated samples before and after heat treatment are shown in **Figure 4**. As expected from the splat morphology, the SEM images of the Y_2O_3 coatings (Figure 4a) show a dense and homogenous coating microstructure. Only few pores can be observed. After heat treatment, no signs of delamination are observed. In contrast to this, the YSZ coatings offer a more inhomogeneous coating microstructure with a fine distributed porosity (Figure 4b). As a result of the bad contact between coating and substrate, the coating was partly delaminated even in the as-sprayed state. After furnace cycling, the coating was completely delaminated. The SEM images of the $Gd_2Zr_2O_7$ coatings (Figure 4c) reveal dense and homogenous coating microstructures. Although the analysis of the splats

suggested otherwise, the coating seems to adhere to the substrate. After heat treatment, a gap between coating and substrate is observed and the coating is partly delaminated.

A closer view at the Y_2O_3 coating–substrate interface before and after thermal cycling is shown in **Figure 5**. The formation of a continuous reaction scale can be observed at the interface. This reaction scale is present directly after spraying and grows during furnace cycling. After furnace cycling, a thickness of about 0.3 µm is reached. The formation of three different phases was observed. Based on the Y_2O_3–Al_2O_3 phase diagram[52] and the findings of Mechnich et al.,[23] it is assumed that these are $YAlO_3$, $Y_3Al_5O_{12}$, and $Y_4Al_2O_9$. Mechnich et al.[23] showed the formation of these phases at the Al_2O_3–Y_2O_3 interface after annealing. In this study, we can show that the reaction of Y_2O_3 with Al_2O_3 starts already during the coating process. This is in accordance with our study concerning VLPPS-$YAlO_3$ coatings.[26] The formation of a reaction layer in the as-sprayed state can be explained by the high substrate temperature during coating and the good wetting of Y_2O_3 splats. The yttrium aluminates, which are formed at the interface, have similar CTEs, compared with coating and substrate; therefore, coating failure due to the formation of a reaction layer is not expected. In the study by Mechnich et al.,[23] it was also assumed that the reaction layer could lead to an improvement in adhesion in this special case. In contrast, no mixing phase is known from the Al_2O_3–ZrO_2 phase diagram.[30] As the formation of a reaction phase at the interphase is not expected, it can be assumed that the adhesion of YSZ is based on mechanical interlocking and is not affected by reactions at the interface.

The SEM image of the $Gd_2Zr_2O_7$ coating–substrate interface after heat treatment is shown in **Figure 6**. Even after 80 h at

**ADVANCED
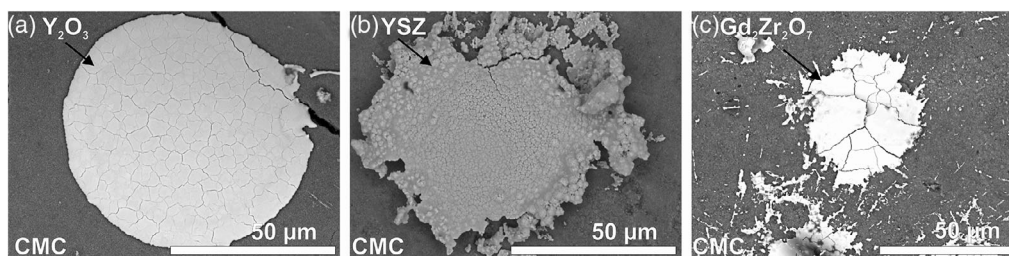SCIENCE NEWS**
www.advancedsciencenews.com

*ADVANCED
ENGINEERING
MATERIALS*
www.aem-journal.com

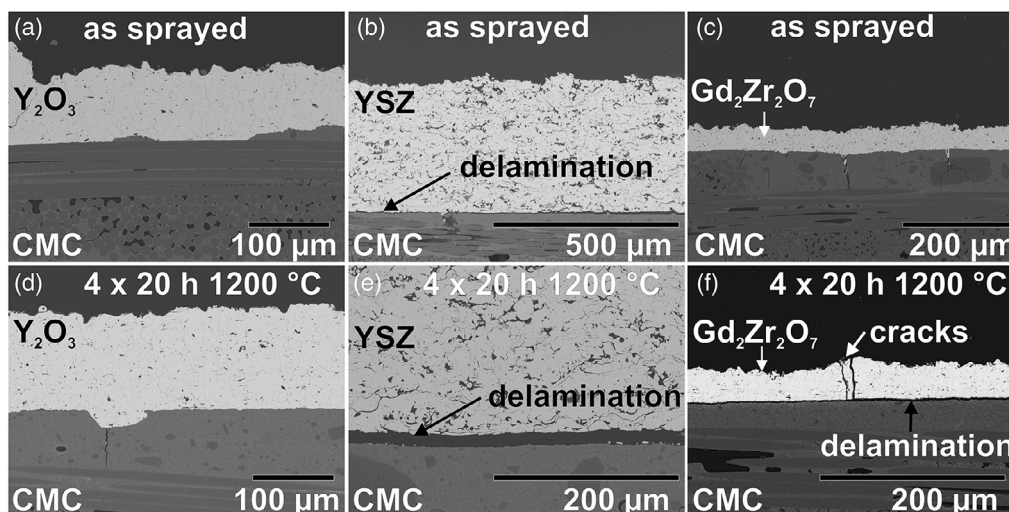**Figure 3.** SEM images of a) Y_2O_3, b) YSZ, and c) $Gd_2Zr_2O_7$ splats on CMC substrates.

Figure 4. SEM images of cross sections of coated CMC substrates without pretreatment. a,d) Y_2O_3 coatings, b,e) YSZ coatings, and c,f) $Gd_2Zr_2O_7$ coatings. Samples in the as-sprayed condition are displayed in parts (a)–(c) and after furnace cycling in parts (d)–(f).
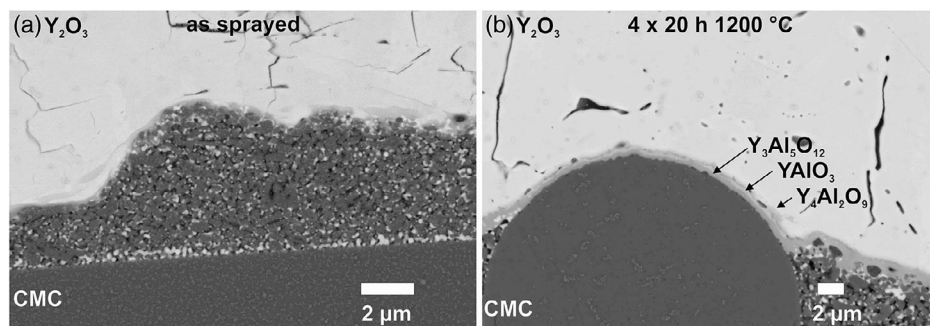

Figure 5. SEM image of the Y_2O_3 coating–substrate interface directly after a) spraying and b) after furnace cycling.

1200 °C, no reaction or diffusion zone can be observed. However, according to the phase diagram[53] and results of Leckie et al.,[29] the reactions of $Gd_2Zr_2O_7$ with Al_2O_3 are likely. Leckie et al.[29] reported a reaction between EB-PVD-$Gd_2Zr_2O_7$ coatings and Al_2O_3 substrates, leading to the formation of $GdAlO_3$ and $Gd_4Al_2O_9$ at the interface. The absence of a reaction layer in our experiments might be explained by poor contact between coating and substrate, which slows the diffusion. The SEM image of the $Gd_2Zr_2O_7$ splat (Figure 3c) supports this assumption. The partly delamination of splats hinders interdiffusion and the formation of a reaction layer between coating and substrate. The

quite high CTE mismatch between coating and substrate ($\Delta_{CTE} \simeq 3.9 \times 10^{-6} \, K^{-1}$) is another driving force for coating spallation and thus prevents the formation of a reaction layer.

3.2. Coating Formation on Laser Structured Surfaces

Two different structures were chosen for surface pretreatment: mixed structure and dot structure.[31] The surface structures of both are shown in **Figure 7**. The so-called mixed structure comprises an irregular wavy and rough surface. In contrast to
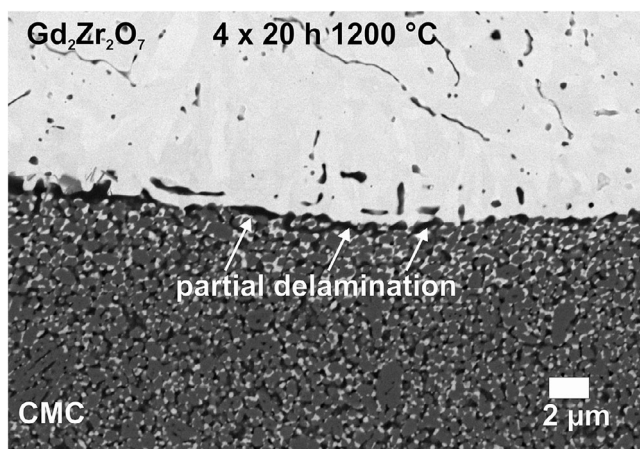
**ADVANCED
SCIENCE NEWS**
www.advancedsciencenews.com

**ADVANCED
ENGINEERING
MATERIALS**
www.aem-journal.com

Figure 6. SEM image of $Gd_2Zr_2O_7$ coating–substrate interface after thermal cycling.

this, the dot structure offers a regular surface profile with valleys in defined distances and parts of the untreated surface can be found in between. The initial surface roughness of untreated samples was $R_a = 2.6\,\mu m$. Surface structuring by laser ablation could increase the surface roughness, a value of $R_a = 3.9\,\mu m$ was measured for the dot structure. A significant increase to $R_a = 17.5\,\mu m$ was achieved for the mixed structure. Nevertheless, both generated structures should offer manifold possibilities for the mechanical interlocking of the coating. Furthermore, the cavities and bumps of the surface are obstacles at which cracks can be deflected or stopped.[54–56] Both effects contribute to an increased coating adhesion.

The formation of a reaction layer between Y_2O_3 coating and the untreated Al_2O_3 substrate did not lead to delamination. On the contrary, the reaction is a sign of good contact between coating and substrate. The presence of a reaction layer indicates that interdiffusion must have occurred at the interface. Because covalent and ionic bonds are the strongest attractive forces, the reaction between coating and substrate helps to promote adhesion and outweighs the effect of interdiffusion.[57] As a consequence, a good adhesion strength during tensile tests and burner-rig tests is expected. SEM images of the structured surfaces coated with Y_2O_3 are shown in **Figure 8**a,b. It can be clearly seen that the coating was able to infiltrate the cavities. Again, the Y_2O_3 coatings exhibit good adhesion. A homogenous coating microstructure is observed with no signs of delamination after furnace cycling.

In contrast to YSZ coatings on untreated CMC substrates, the YSZ coatings on laser structured CMC substrates did not fail during furnace cycling. However, the SEM images (Figure 8c,d) reveal that the coatings on dot-structured samples show partly delamination on the untreated parts of the CMC after furnace cycling. At the same time, the coating seems to be still adherent to the substrate in the laser-generated cavities. No delamination cracks can be observed in the SEM image of the YSZ coating on the substrate with the mixed structure. The higher surface roughness seems to offer enough possibilities for clamping and therefore significantly increases the adhesion.

The SEM images of the cross sections of the $Gd_2Zr_2O_7$-coated samples in the as-sprayed state and after heat treatment are shown in Figure 8e,f. The bonding of the $Gd_2Zr_2O_7$ coatings seems to be improved on the laser pretreated substrates. In contrast to the coatings on untreated substrates, there are no signs of delamination in the coating systems on structured substrates. The coating–substrate interface looks still intact, even after furnace cycling.

3.3. Pull-Off Adhesion and Burner-Rig Performance

To analyze the adhesion properties of the different coating materials on structured and unstructured CMC substrates, PATs and burner-rig tests were conducted. The test results are shown in **Figure 9**. For better orientation, the lower limit of the average cohesion strength of the CMC substrate ($8.8 \pm 1.1\,MPa$) was added. The pull-off adhesion tests of the Y_2O_3 coatings revealed that the adhesion of these coatings is so strong that all coatings had a higher adhesion strength than the CMC itself. The slight increase in the adhesion strength by previous laser structuring of the substrate is not significant in this system, as the measured strength exceeds the average strength of the Al_2O_3/Al_2O_3 CMC. Furthermore, the failure occurred within the CMC or the coating, not at the coating–substrate interface. This leads to the conclusion that the coating–substrate interface is stronger than the cohesion within the substrate and the coating itself.

In contrast to this, the YSZ and $Gd_2Zr_2O_7$ coatings on untreated substrates failed directly after the beginning of the test. The failure occurred directly at the coating–substrate interface. This result corresponds to the weak coating adhesion and poor wetting of these coatings on untreated substrates, which were discussed previously. The YSZ coating on the dot-structured substrate also failed immediately. This result is quite surprising, as the furnace cycling of these samples suggested a better adhesion. However, the dot-structured CMC was not able to increase the adhesion strength and the delamination occurred directly at
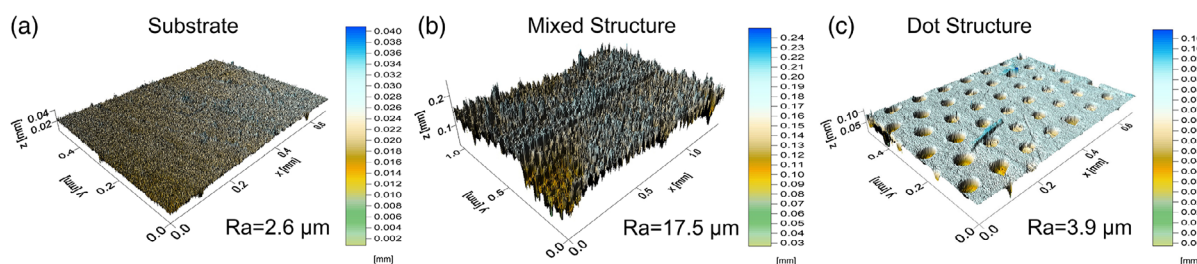

Figure 7. White light topography image of different surface structures: a) untreated substrate, b) mixed structure, and c) dot structure.
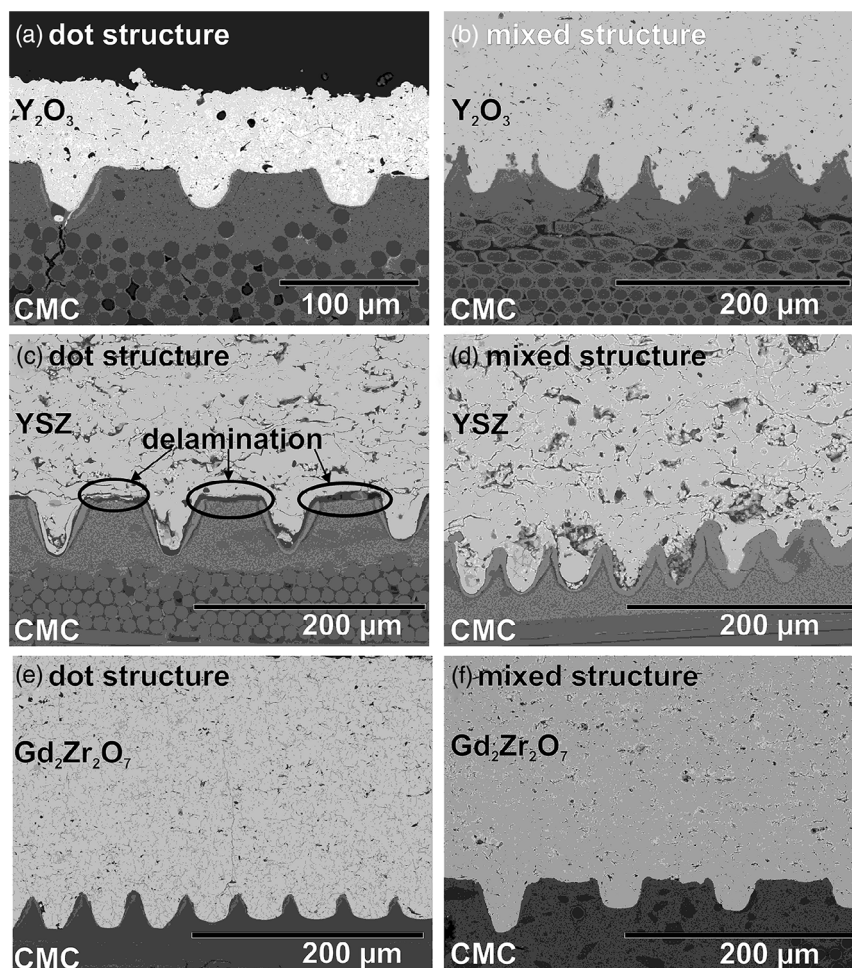
**ADVANCED
SCIENCE NEWS**

www.advancedsciencenews.com

**ADVANCED
ENGINEERING
MATERIALS**

www.aem-journal.com

Figure 8. SEM images of a,b) Y_2O_3, c,d) YSZ, and e,f) $Gd_2Zr_2O_7$ coatings on Al_2O_3/Al_2O_3-CMC substrates after furnace cycling (4 × 20 h at 1200 °C). Samples with dot surface structure are displayed in parts (a), (c), and (e), and samples with the mixed surface structure are displayed in parts (b), (d), and (f).

the interface, as already indicated in the furnace cycling experiments. This might be attributed to the large untreated parts between the dots, where insufficient contact between coating and substrate prevails. The measurements show that the adhesion strength of YSZ coatings on the mixed structured substrate was significantly increased. The increased adhesion strength at the interface changed the failure mechanism from failure at the interface to failure within the coating.

In case of the $Gd_2Zr_2O_7$ coatings, the adhesion strength could be drastically increased by laser pretreatment of the substrate. The measured adhesion strength is in the range of the cohesion strength of the substrate itself and the failure mode was shifted to the inner part of the CMC. The increased adhesion strength is in accordance with the furnace cycling results discussed in the section mentioned previously.

The burner-rig tests confirm these results. Tests with Y_2O_3 coatings were stopped after 1010 cycles without macroscopic failure. This lifetime corresponds to the average number of cycles reached for state-of-the-art YSZ TBC systems in this rig (shown in yellow in Figure 9b). The SEM images of the Y_2O_3 coatings (Figure 9c–e) show that all coatings are still well-

adherent so that a significantly longer lifetime can be expected. After about an 80 h burner-rig testing, the reaction scale showed a similar thickness after 80 h of furnace cycling. This indicates that the reaction scale at the interface is thermodynamically and mechanically stable and thus promotes adhesion.

The YSZ coating on the untreated substrate failed after 648 cycles. Considering the weak adhesion and the fact that the coating was already partly delaminated after spraying (Figure 4), this lifetime is surprisingly long. A significantly longer lifetime was observed for the coating on the dot-structured sample (1730 cycles). Although the pull-off adhesion tests suggest a similar weak adhesion as the coatings on the untreated substrates, the furnace cycling indicates a slightly improved adhesion. The results of the burner-rig tests show that the structuring of the substrate almost triples the lifetime. The loose contact between coating and substrate could allow for compensation of the rather large CTE difference between coating and substrate ($\Delta_{CTE} \simeq 3.2 \times 10^{-6} K^{-1}$), whereas the structuring provides anchor points that prevent delamination. Burner-rig tests of the coating on the mixed structured sample were stopped after 1730 cycles, no macroscopic signs of delamination have
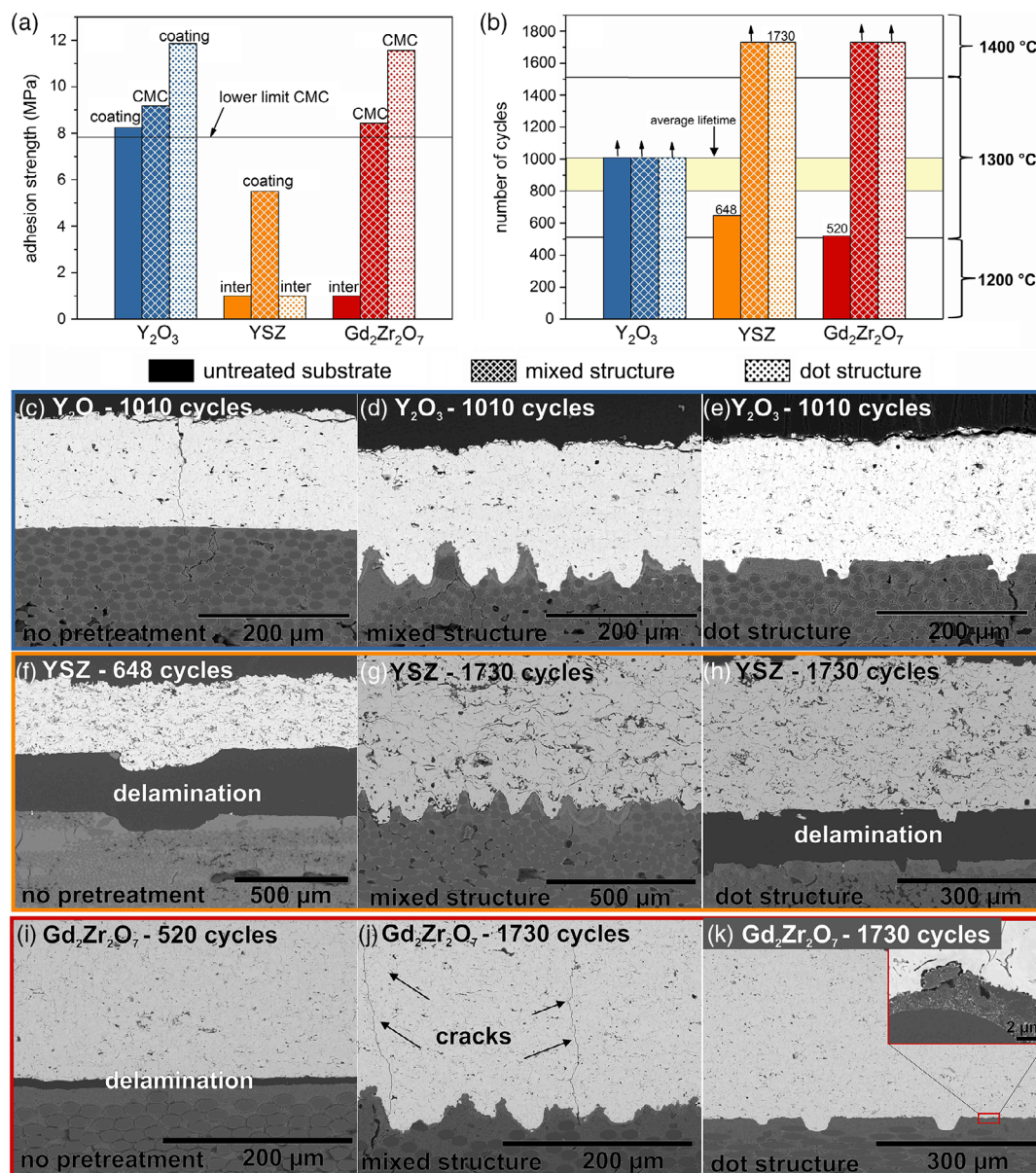
**ADVANCED
SCIENCE NEWS**

www.advancedsciencenews.com

**ADVANCED
ENGINEERING
MATERIALS**

www.aem-journal.com

Figure 9. Results of a) PATs and b) burner-rig test results of Y$_2$O$_3$-coated samples are indicated in blue, YSZ coatings in orange, and results of Gd$_2$Zr$_2$O$_7$ coatings are presented in red. The location of failure is indicated (CMC = within the substrate, coating = failure within the coating, inter = failure at the interface). SEM images of coated samples after burner-rig testing: c–e) Y$_2$O$_3$ coating, f–h) YSZ coating, and i–k) Gd$_2$Zr$_2$O$_7$ coating. Cross sections of coatings on untreated substrates are shown in parts (c), (f), and (i), substrates with mixed structures in parts (d), (g), and (j), and coatings on dot structured samples in parts (e), (h), and (k).

been observed. The SEM image of this sample (Figure 9 f–h) shows that the coating is still well-adherent to the substrate. This is in good agreement with the results of the previous tests. According to the increased adhesion strength, a longer cycling lifetime is expected.

The Gd$_2$Zr$_2$O$_7$ coating on the untreated CMC failed after 520 cycles. The SEM images (Figure 9i) show that delamination took place at the coating–substrate interface. Burner-rig testing of the coatings on the roughened substrates was stopped after 1730 cycles without any failure being detected. The SEM images confirm that no formation of a reaction layer or delamination

cracks occurred. Some vertical cracks can be observed in the coating on the substrate with the mixed structure. These cracks seem to be generated at the interface and spread toward the coating surface. The reason for the formation of the cracks is probably the large CTE difference ($\Delta_{CTE} \simeq 3.9 \times 10^{-6}\,K^{-1}$) between coating and substrate, leading to tensile stresses within the Gd$_2$Zr$_2$O$_7$ coating during cooling. The thermal gradients occurring during thermal cycling ($\Delta_T = 600\,°C$) additionally reinforce these stresses. The lack of these cracks in the coatings on the dot structured samples might be explained by the looser contact between coating and substrate in this system.

4. Conclusion

The adhesion mechanisms of different EBCs (Y_2O_3, $Gd_2Zr_2O_7$, and YSZ) on an Al_2O_3/Al_2O_3-CMC were investigated in this study. The coating adhesion was analyzed by means of PATs, furnace cycling tests, and burner-rig tests with thermal gradients. Two different kinds of adhesion were observed: adhesion promoted by chemical bonds between coating and substrate and adhesion promoted by mechanical interlocking.

In case of Y_2O_3 coatings, adhesion is promoted by interdiffusion and formation of a reaction scale between coating and substrate. This layer is formed during plasma spraying and grows during heat treatment to a thickness of about $2\,\mu m$. The formation of chemical bonds leads to a high adhesion strength and the long cycling lifetime of Y_2O_3 coatings on Al_2O_3/Al_2O_3-CMC substrates, even without pretreatment. Based on the results, no statement can be made regarding the question of whether the adhesion can be improved by laser structuring of the substrate. Alongside the already strong adhesion due to the chemical reaction, the surface structuring seems to have a minor effect.

The formation of chemical bonds between coating and substrate was not observed for $Gd_2Zr_2O_7$ and YSZ coatings, although a reaction between Al_2O_3 and $Gd_2Zr_2O_7$ would be possible. The absence of a reaction layer is explained by the slow reaction kinetics and the poor wetting between substrate and coating. Because there are no chemical bonds that promote adhesion, mechanical anchoring is the key mechanism. The untreated substrate is relatively smooth and offers few possibilities for clamping, resulting in weak adhesion of $Gd_2Zr_2O_7$ and YSZ coatings. The substrate surfaces were structured by laser ablation prior to coating to increase the roughness and thus improve the coating adhesion. The results show that surface structuring significantly increases the adhesion and thermal cycling lifetime, which allows the use of those materials in EBC application.

The following conclusions can be made:

1) Coating adhesion strongly depends on the surface structure and wettability of the substrate.

2) Chemical bonds might help to drastically increase the coating adhesion.

3) Bad wetting can suppress the formation of a reaction scale at the interface.

4) If mechanical anchoring is the main adhesion mechanism, surface structuring by laser ablation can significantly increase the adhesion strength and lifetime of the coatings.

Conflict of Interest

The authors declare no conflict of interest.

[1] J. H. Perepezko, *Science* **2009**, *326*, 1068.

[2] Q. Xin, in *Diesel Engine System Design* (Ed: Q. Xin), Woodhead Publishing, Swaston, UK **2013**, pp. 860–908.

[3] J. D. Birchall, *J. Phys. Chem. Solids* **1988**, *49*, 859.

[4] S. Krishnan, J. K. R. Weber, R. A. Schiffman, P. C. Nordine, R. A. Reed, *J. Am. Ceram. Soc.* **1991**, *74*, 881.

[5] N. S. Jacobson, *J. Am. Ceram. Soc.* **1993**, *76*, 3.

[6] D. S. Fox, E. J. Opila, Q. N. Nguyen, D. L. Humphrey, S. M. Lewton, *J. Am. Ceram. Soc.* **2003**, *86*, 1256.

[7] E. J. Opila, D. L. Myers, *J. Am. Ceram. Soc.* **2004**, *87*, 1701.

[8] M. Fritsch, *Heißgaskorrosion keramischer Werkstoffe in H2O-haltigen Rauchgasatmosphären*, Fraunhofer IRB Verlag, TU Dresden, Germany **2007**.

[9] M. Fritsch, H. Klemm, *J. Eur. Ceram. Soc.* **2008**, *28*, 2353.

[10] M. Fritsch, H. Klemm, *Ceram. Eng. Sci. Proc.* **2006**, *27*, 149.

[11] M. Fritsch, H. Klemm, M. Herrmann, B. Schenk, *J. Eur. Ceram. Soc.* **2006**, *26*, 3557.

[12] M. Herrmann, H. Klemm, *Comprehens. Hard Mater.* **2014**, *2*, 413.

[13] E. Bakan, D. Marcano, D. Zhou, Y. J. Sohn, G. Mauer, R. Vaßen, *J. Thermal Spray Technol.* **2017**, *26*, 1011.

[14] B. T. Richards, H. N. G. Wadley, *J. Eur. Ceram. Soc.* **2014**, *34*, 3069.

[15] Pritzkow Oxidkeramischer Faserverbundwerkstoff "Keramikblech", Neuentwicklungen für den Einsatz bis 1300 °C, https://www.keramikblech.com/fileadmin/user_upload/pdf/Neuentwicklungen.pdf

[16] C. Gatzen, D. E. Mack, O. Guillon, R. Vaßen, *J. Am. Ceram. Soc.* **2019**, *102*, 6850.

[17] M. Takeuchi, T. Kato, K. Hanada, T. Koizumi, S. Aose, *J. Phys. Chem. Solids* **2005**, *66*, 521.

[18] E. Courcot, F. Rebillat, F. Teyssandier, C. Louchet-Pouillerie, *J. Eur. Ceram. Soc.* **2010**, *30*, 1903.

[19] M. Fritsch, H. Klemm (Fraunhofer Gesellschaft), DE102006030235A1.

[20] E. I. Zoz, E. N. Fomichev, A. A. Kalashnik, G. G. Eliseeva, *Russ. J. Inorg. Chem.* **1982**, *27*, 54.

[21] D. Zhu, D. S. Fox, N. P. Bansal, R. A. Miller, *Advanced Oxide Material Systems for 1650 °C Thermal/Environmental Barrier Coating Applications*, NASA/TM–2004-213219A, Hanover, MD **2004**.

[22] X. Zhou, Z. Xu, X. Fan, S. Zhao, X. Cao, L. He, *Mater. Lett.* **2014**, *134*, 146.

[23] P. Mechnich, W. Braue, *J. Eur. Ceram. Soc.* **2013**, *33*, 2645.

[24] T. Behrendt, S. Hackemann, P. Mechnich, Y. Shi, S. Hönig, S. Hofmann, D. Koch, *J. Eng. Gas Turbines Power* **2017**, *139*, 031507.

[25] P. Mechnich, W. Braue, H. Schneider, *Int. J. Appl. Ceram. Technol.* **2004**, *1*, 343.

[26] C. Gatzen, D. E. Mack, O. Guillon, R. Vaßen, *Coatings* **2019**, *9*, 609.

[27] C. M. Weyant, K. T. Faber, *Surf. Coat. Technol.* **2008**, *202*, 6081.

[28] R. Vaßen, F. Traeger, D. Stöver, *Int. J. Appl. Ceram. Technol.* **2004**, *1*, 351.

[29] R. M. Leckie, S. Krämer, M. Rühle, C. G. Levi, *Acta Mater.* **2005**, *53*, 3281.

[30] S. Lakiza, O. Fabrichnaya, C. Wang, M. Zinkevich, F. Aldinger, *J. Eur. Ceram. Soc.* **2006**, *26*, 233.

[31] C. Gatzen, D. E. Mack, O. Guillon, R. Vaßen, *J. Laser Appl.* **2019**, *31*, 022018.

[32] R. Vaßen, E. Bakan, C. Gatzen, S. Kim, D. Mack, O. Guillon, *Coatings* **2019**, *9*, 784.

[33] M. Gerendás, Y. Cadoret, C. Wilhelmi, T. Machry, R. Knoche, T. Behrendt, T. Aumeier, S. Denis, J. Göring, D. Koch, K. Tushtev, *ASME Turbo Expo.* **2011**, *1*, 477.

[34] W. Braue, P. Mechnich, *Schutzschichtkonzepte für oxidische Faserverbundwerkstoffe*, Werkstoff-Kolloquium, Köln-Porz **2004**.

[35] P. Mechnich, W. Braue, in *Design, Development, and Applications of Engineering Ceramics and Composites*, John Wiley & Sons, Inc., New York **2010**, pp. 285–293.

[36] W. Braue, P. Mechnich, D. J. Green, *J. Am. Ceram. Soc.* **2011**, *94*, 4483.

[37] P. Mechnich, W. Braue, H. Schneider, *Int. J. Appl. Ceram. Technol.* **2004**, *1*, 343.

[38] D. Wang, Y. Guo, K. Liang, K. Tao, *Sci. China Ser. A Math.* **1999**, *42*, 80.

[39] D. K. Smith, W. Newkirk, *Acta Crystallograph.* **1965**, *18*, 983.

[40] B. Mandal, A. Jain, V. Sathe, S. Deb, A. K. Tyagi, *J. Solid State Chem.* **2007**, *180*, 2643.

[41] M. G. Paton, E. N. Maslen, *Acta Crystallograph.* **1965**, *19*, 307.

[42] F. Traeger, R. Vaßen, K.-H. Rauwald, D. Stöver, *Adv. Eng. Mater.* **2003**, *5*, 429.

[43] F. X. Zhang, M. Lang, J. W. Wang, U. Becker, R. C. Ewing, *Phys. Rev. B* **2008**, *78*, 064114.

[44] B. Bondars, G. Heidemane, J. Grabis, K. Laschke, H. Boysen, J. Schneider, F. Frey, *J. Mater. Sci.* **1995**, *30*, 1621.

[45] J. Zhang, H. Cui, P. Zhu, C. Ma, X. Wu, H. Zhu, Y. Ma, Q. Cui, *J. Appl. Phys.* **2014**, *115*, 023502.

[46] E. Bakan, D. E. Mack, G. Mauer, R. Vaßen, *J. Am. Ceram. Soc.* **2014**, *97*, 4045.

[47] M. Mutter, G. Mauer, R. Mücke, O. Guillon, R. Vaßen, *Surf. Coat. Technol.* **2017**, *318*, 157.

[48] P. L. Fauchais, J. V. R. Heberlein, M. I. Boulos, *Thermal Spray Fundamentals*, Springer, New York, **2014**.

[49] A. A. Syed, A. Denoirjean, B. Hannoyer, P. Fauchais, P. Denoirjean, A. A. Khan, J. C. Labbe, *Surf. Coat. Technol.* **2005**, *200*, 2317.

[50] M. Fukumoto, E. Nishioka, T. Matsubara, *Surf. Coat. Technol.* **1999**, *120–121*, 131.

[51] R. B. Heimann, *Plasma-Spray Coating*, Weinheim VCH, New York, **1996**.

[52] O. Fabrichnaya, H. J. Seifert, T. Ludwig, F. Aldinger, A. Navrotsky, *Scand. J. Metall.* **2001**, *30*, 175.

[53] O. Fabrichnaya, H. J. Seifert, *J. Phase Equilibr. Diffus.* **2010**, *32*, 2.

[54] R. Kromer, S. Costil, J. Cormier, L. Berthe, P. Peyre, D. Courapied, *J. Thermal Spray Technol.* **2016**, *25*, 401.

[55] W. Nowak, D. Naumenko, G. Mor, F. Mor, D. E. Mack, R. Vassen, L. Singheiser, W. J. Quadakkers, *Surf. Coat. Technol.* **2014**, *260*, 82.

[56] W. X. Zhang, X. L. Fan, T. J. Wang, *Appl. Surf. Sci.* **2011**, *258*, 811.

[57] A. J. Kinloch, *Adhesion and Adhesives*, Springer, Dordrecht, **1987**.

2000087 (10 of 10)